Vol 455|25 September 2008|doi:10.1038/nature07288

LETTERS

Reconstruction of non-classical cavity field states with snapshots of their decoherence

Samuel Deléglise[1], Igor Dotsenko[1,2], Clément Sayrin[1], Julien Bernu[1], Michel Brune[1], Jean-Michel Raimond[1] & Serge Haroche[1,2]

The state of a microscopic system encodes its complete quantum description, from which the probabilities of all measurement outcomes are inferred. Being a statistical concept, the state cannot be obtained from a single system realization, but can instead be reconstructed[1] from an ensemble of copies through measurements on different realizations[2–4]. Reconstructing the state of a set of trapped particles shielded from their environment is an important step in the investigation of the quantum–classical boundary[5]. Although trapped-atom state reconstructions[6–8] have been achieved, it is challenging to perform similar experiments with trapped photons because cavities that can store light for very long times are required. Here we report the complete reconstruction and pictorial representation of a variety of radiation states trapped in a cavity in which several photons survive long enough to be repeatedly measured. Atoms crossing the cavity one by one are used to extract information about the field. We obtain images of coherent states[9], Fock states with a definite photon number and 'Schrödinger cat' states (superpositions of coherent states with different phases[10]). These states are equivalently represented by their density matrices or Wigner functions[11]. Quasi-classical coherent states have a Gaussian-shaped Wigner function, whereas the Wigner functions of Fock and Schrödinger cat states show oscillations and negativities revealing quantum interferences. Cavity damping induces decoherence that quickly washes out such oscillations[5]. We observe this process and follow the evolution of decoherence by reconstructing snapshots of Schrödinger cat states at successive times. Our reconstruction procedure is a useful tool for further decoherence and quantum feedback studies of fields trapped in one or two cavities.

Engineering and reconstructing non-classical states of trapped light requires cavities that prevent the escape of even single photons during the preparation and read-out procedures. We have built a cavity made of highly reflecting superconducting mirrors[12] whose long damping time, $T_c = 0.13$ s, allows the trapped field to interact with thousands of atoms crossing the cavity one by one. The interaction with atoms is used to turn an initial coherent field into a Fock or Schrödinger cat state and, subsequently, to reconstruct it. An ensemble of trapped photons becomes, like a collection of trapped atoms, an 'object of investigation' to be manipulated and observed for fundamental tests and quantum information purposes.

Our set-up is sketched in Fig. 1a. The cavity C, resonant at 51 GHz, is cooled to a temperature of 0.8 K (mean number of residual blackbody photons, $n_b = 0.05$). A coherent microwave field with a Poisson photon number distribution (mean, n_m; standard deviation, $\Delta n = \sqrt{n_m}$) is initially injected into C using a classical pulsed source S. Rubidium atoms from an atomic beam are prepared, in box B, in the circular Rydberg state with principal quantum number 50 ($|g\rangle$). The cavity is detuned from the transition between $|g\rangle$ and the adjacent circular state with principal quantum number 51 ($|e\rangle$) by an amount δ, precluding atom–field energy exchange. The pulsed atom preparation produces Rydberg atoms with a velocity of 250 m s^{-1}. Auxiliary microwave cavities R_1 and R_2 sandwiching C are connected to a microwave source S′. They are used to apply resonant pulses to the atoms. The R_1 pulse performs the $|g\rangle \rightarrow (|e\rangle + |g\rangle)/\sqrt{2}$ transformation. The same pulse, differing by an adjustable phase shift ϕ, is applied in R_2. Atoms are counted by the detector D, discriminating $|e\rangle$ and $|g\rangle$ (one atom on average every 0.5 ms). For experimental details, see refs 13 and 14.

The R_1–R_2 combination forms a Ramsey interferometer[14]. It is sensitive to the atomic-state-superposition phase shift induced by the atom's interaction with the field in C, which is characterized by

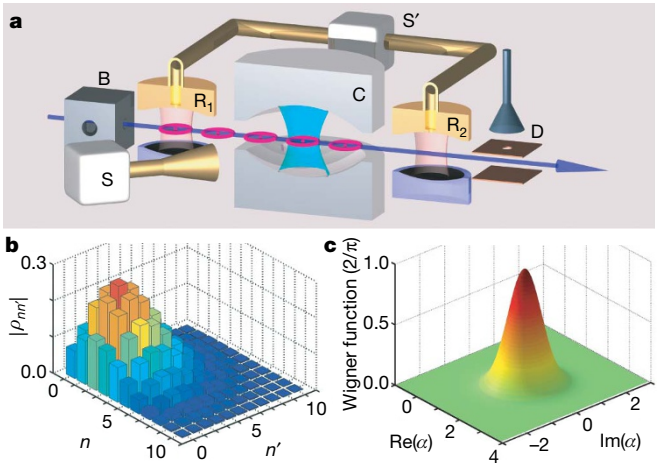

Figure 1 | Reconstructing a coherent state. a, The set-up, showing the stream of atoms prepared in box B and crossing the R_1–R_2 interferometer in which the cavity C, made of two mirrors facing each other, is inserted. The source S, coupled to a waveguide, generates a coherent microwave pulse irradiating C on one side. By diffraction at the mirrors' edges, it injects into C a small coherent field with controlled amplitude and phase. The field outside vanishes almost instantaneously when S is switched off. The source S is used to prepare an initial field in C and, later, to translate the field for state reconstruction. Another pulsed source, S′, feeds the interferometer cavities R_1 and R_2. Information is extracted from the field by state-selective atomic counting in D. **b**, Density matrix (modulus of matrix elements) of a coherent state of amplitude $\beta = \sqrt{2.5}$, reconstructed in an 11-dimensional Hilbert space. The reconstruction parameters are $\delta/2\pi = 65$ kHz and $\phi = -\Phi(0, \delta) + \pi$. We sample 161 points in phase space and for each point detect ~7,000 atoms over 600 realizations. The fidelity, $F = \langle\beta|\rho|\beta\rangle$, of the reconstructed state is 0.98. **c**, Wigner function (in units of $2/\pi$) obtained from the density matrix shown in **b**.

[1]Laboratoire Kastler Brossel, Ecole Normale Supérieure, CNRS, Université Pierre et Marie Curie, 24 rue Lhomond, 75231 Paris Cedex 05, France. [2]Collège de France, 11 place Marcelin Berthelot, 75231 Paris Cedex 05, France.

the Rabi frequency $\Omega/2\pi = 49$ kHz. This phase shift is described by an operator $\Phi(N,\delta)$ that depends on δ and the photon number operator $N = a^\dagger a$ (where a and $a^\dagger$ respectively denote the photon annihilation and creation operators). To lowest order, $\Phi(N,\delta)$ is linear in N, but for the small δ/Ω values of our experiment, we take into account its exact nonlinear expression[13]. The interferometer measures $\cos(\Phi(N,\delta)+\phi)$, which is sensitive to the diagonal elements of the field density matrix in the Fock state basis, but contains no information about the coherences between these states. To obtain this information, we measure the phase shifts produced by the field after it has been translated in phase space, by mixing it with reference coherent fields of adjustable complex amplitudes α. These translations, described by the operators $D(\alpha) = \exp(\alpha a^\dagger - \alpha^* a)$ (where the asterisk denotes complex conjugation), are achieved by injecting a second field pulse into C.

We denote by ρ the density matrix of the field to be reconstructed (Fock-state-basis matrix elements, $\rho_{nn'}$), by $\rho^{(\alpha)} = D(\alpha)\rho D(-\alpha)$ the density matrix after field translation and by P_e and P_g the respective probabilities of finding in $|e\rangle$ and $|g\rangle$ the first atom that crosses the interferometer (experimentally obtained by averaging over many field realizations). The difference $P_e - P_g = \mathrm{Tr}[\rho^{(\alpha)}\cos(\Phi(N,\delta)+\phi)]$ is the expectation value in the translated state of the diagonal field operator $\cos(\Phi(N,\delta)+\phi)$. The measurement is non-demolition for the photon number[15], and the ensemble average of first-crossing atoms does not change $\rho^{(\alpha)}_{nn}$. Hence, the same $P_e - P_g$ expression holds for the second (or any subsequent) atom. We thus determine $P_e - P_g$ by averaging the detections of successive atoms for a single field realization with those measured for different realizations. A measuring sequence for each realization lasts 4 ms, which is short in comparison with the characteristic evolution time of the state. We also correct the raw $P_e - P_g$ values by taking into account the known imperfections of the interferometer.

The $P_e - P_g$ difference is also the expectation value of $G(\alpha,\phi,\delta) = D(-\alpha)\cos(\Phi(N,\delta)+\phi)D(\alpha)$ in state ρ. By sampling α values, we obtain the expectations $g(\alpha,\phi,\delta)$ of an ensemble of non-commuting $G(\alpha,\phi,\delta)$ operators satisfying:

$$\mathrm{Tr}[\rho G(\alpha,\phi,\delta)] = g(\alpha,\phi,\delta) \quad (1)$$

Provided that we sample a large enough number of points α in phase space, equation (1) allows us to reconstruct ρ. To ensure that the reconstructed state does not contain any information other than that extracted from the data, we also maximize the field entropy, $-\mathrm{Tr}[\rho\ln\rho]$, during the reconstruction procedure (principle of maximum entropy[16]).

The Wigner function associated with the state described by the density matrix ρ is defined at point α in phase space as[14]

$$W(\alpha) = \frac{2}{\pi}\mathrm{Tr}[D(-\alpha)\rho D(\alpha)e^{i\pi N}] \quad (2)$$

and (to within a normalization) is the expectation value of the photon number parity operator $\exp(i\pi N)$ in the state translated by $-\alpha$. The Wigner function could be determined directly[17] if the atoms underwent an exact phase shift of π per photon, realizing the measurement of $\exp(i\pi N)$ after field translation by different values of α. This would be a special case of reconstruction corresponding to $\Phi(N,\delta) - \Phi(0,\delta) = \pi N$. This relation cannot be satisfied, owing to nonlinear atom–field phase shift. Instead of a direct determination of the Wigner function, we thus reconstruct ρ first and then obtain the Wigner function using equation (2).

Figure 1b shows the reconstructed density matrix of a coherent state. Along its diagonal, we recognize the Poisson photon number distribution ρ_{nn}. The off-diagonal elements describe the classical coherence of the state. The corresponding Wigner function, shown in Fig. 1c, is, as expected, a Gaussian peak with a circular symmetry.

As a first non-classical example, we have reconstructed Fock states. To generate them, we prepare a coherent field and let it interact with atoms, achieving a quantum non-demolition measurement of the photon number that progressively projects the field onto a Fock state $|n_0\rangle$. This procedure is adapted from ref. 15, taking into account the known effect of cavity damping during state projection. Following this preparation, we apply our reconstruction method with subsequent probe atoms and reconstruct the Fock states present in the expansion of the initial coherent state.

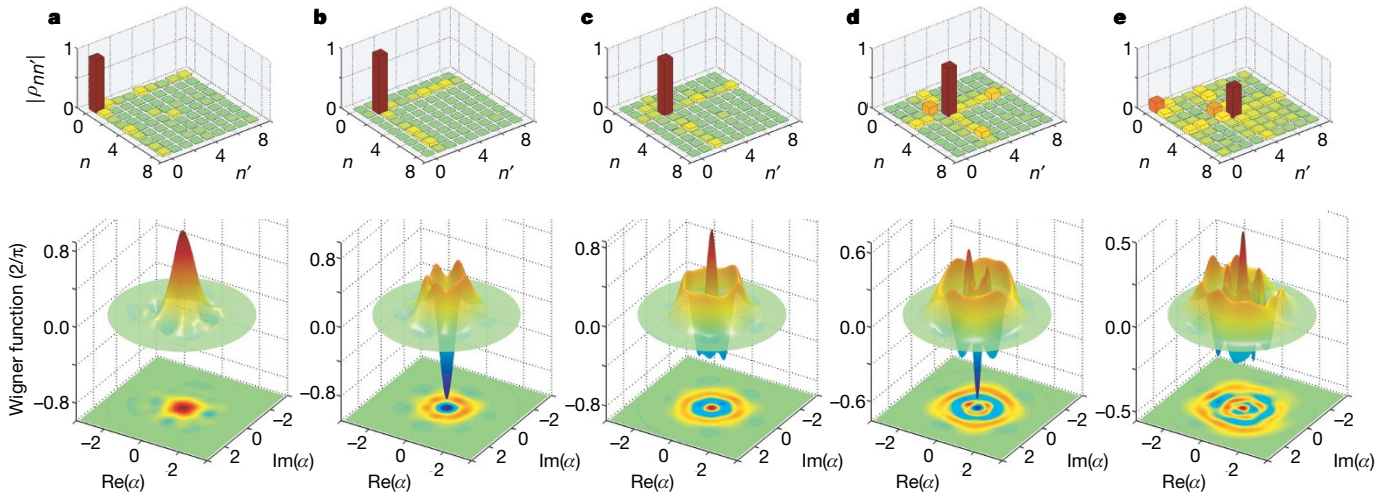

Figure 2 | Reconstructing Fock states. a–e, Reconstructed density matrices (modulus of matrix elements) and Wigner functions (in units of $2/\pi$) of the $n_0 = 0, 1, 2, 3, 4$ Fock states prepared by quantum non-demolition projection of an initial coherent field ($n_m = 1.5$ for $n_0 = 0, 1, 2, 3$; $n_m = 5.5$ for $n_0 = 4$). The Wigner functions are shown as three-dimensional plots and two-dimensional projections. We select a photon number n_0 if, after the detection of ~60 preparation atoms, the measurement has converged to a Fock state having a probability >0.9 for $n_0 = 0, 1, 2, 3$ and >0.8 for $n_0 = 4$. The same detuning ($\delta/2\pi = 120$ kHz) is used for state preparation and reconstruction, corresponding to $\partial\Phi/\partial n \approx \pi/2$ at $n = 3$. Two values of ϕ ($-\Phi(0,\delta)+\pi$ and $-\Phi(0,\delta)+\pi/2$) are used for state preparation and reconstruction, which is made in a nine-dimensional Hilbert space. We sample ~400 points in phase space and, for each point, average between about 50 (for $n_0 = 3$) and 500 ($n_0 = 0, 1$) realizations, with ~10 atoms in each realization. In addition to the main peak in the density matrices, for $n_0 > 1$ we observe a small diagonal peak at $n = n_0 - 1$ due to cavity damping during reconstruction. A peak at $n = 0$ also appears in the $n_0 = 4$ density matrix, because of imperfections in the state preparation process that selects the photon number modulo four (as $\Phi(n+4,\delta) \approx \Phi(n,\delta) + 2\pi$). The off-diagonal elements in the density matrices and the corresponding fluctuations in the angular distributions of the Wigner functions mainly reflect statistical noise (fewer atoms detected for reconstructing $n_0 = 2, 3, 4$ than for $n_0 = 0, 1$). The fidelities, $F = \langle n_0|\rho|n_0\rangle$, of the reconstructed states are 0.89, 0.98, 0.92, 0.82, 0.51 for $n_0 = 0, 1, 2, 3, 4$, respectively.

Figure 2 displays the obtained density matrices together with the corresponding Wigner functions for $n_0 = 0$ (vacuum), 1, 2, 3, 4. As expected, the density matrices mainly exhibit a single diagonal peak. Each Wigner function shows circular rings around the origin of phase space, where it is positive for even n_0 and negative for odd n_0. The number of rings and their size increases as expected with n_0. Photonic Fock states with small values of n_0 have already been reconstructed in free space[18–20] and in a cavity[21], but to our knowledge this is the first Fock state reconstruction with $n_0 > 2$.

To generate a Schrödinger cat state[22], we first inject into C a coherent field of amplitude $\beta = \sqrt{n_m}$. We then prepare an atom in the state $(|e\rangle + |g\rangle)/\sqrt{2}$ using R_1 and send it into C. The two atomic components shift the phase of the field in opposite directions. Neglecting atom–field phase shift nonlinearity, the field is split into two coherent states of complex amplitudes $\beta\exp(\pm i\chi)$, where $\chi = (\partial\Phi(n,\delta)/\partial n)/2$ evaluated at $n = n_m$. The atom is entangled with the field in the state $(|e\rangle|\beta\exp(i\chi)\rangle + |g\rangle|\beta\exp(-i\chi)\rangle)/\sqrt{2}$. The R_2 pulse then mixes $|e\rangle$ and $|g\rangle$ again. Last, the atomic detection, depending upon its outcome ($|g\rangle$ or $|e\rangle$), projects the field onto one of the two Schrödinger cat states $(|\beta\exp(i\chi)\rangle \pm |\beta\exp(-i\chi)\rangle)/\sqrt{2}$. We call these 'even' (plus sign) and 'odd' (minus sign) Schrödinger cat states because they contain, for $\chi = \pi/2$, only even and odd photon numbers, respectively. After this preparation, we apply our reconstruction procedure.

Figure 3a, b shows the Wigner functions of the even and odd Schrödinger cat states obtained from the same coherent field ($n_m = 3.5$, $\chi = 0.37\pi$). They exhibit two well-separated positive peaks that are associated with the classical components and whose slightly elongated shapes are due to the phase shift nonlinearity neglected above. The 'size' of each of these states, defined as the squared distance between the peaks (and expressed as a number of photons), is $d^2 \approx 4n_m\sin^2\chi = 11.8$ photons. Between these peaks, oscillating features with alternating positive and negative values are the signatures of the state's quantum interference. The even and odd Schrödinger cat states have nearly identical classical components and only differ in the sign of their quantum interferences. The theoretical Wigner functions, taking the nonlinearity in the preparation of the Schrodinger cat states into account, are shown for comparison in the insets. The fidelity of the two states (overlap between the reconstructed ρ and the expected ρ) is $F = 0.72$. It is mainly limited by imperfections in the R_1 and R_2 pulses applied to the preparation atom, which reduce the contrast of the quantum interference feature. If the preparing atom is detected without discriminating $|e\rangle$ and $|g\rangle$, we obtain the statistical mixture of even and odd Schrödinger cat states whose Wigner function is shown in Fig. 3c. Equivalently, this is a statistical mixture of the two classical components. Although non-classical states of propagating light with similar Wigner functions have previously been observed[23], here well-separated classical components of a field can be identified in a reconstructed state and unambiguously distinguished from their quantum interference term.

Schrödinger cats states are model states for exploring decoherence, the phenomenon accounting for the transition between quantum and classical behaviours[5]. Our reconstruction method allows us to study this process. Immediately after state preparation, we realize the $D(\alpha)$ translation and detect a sequence of atoms divided into 4-ms time windows. These atoms record $P_e - P_g$ as a function of time, without modifying the dynamics of this quantity. We average the results of realizations corresponding to the same translation and time window, and then repeat the process for different values of α. This provides a direct record of the evolution of the translated states, rather than that of the state itself. The two dynamics are closely related, however. Decoherence acting on the initial density operator $\rho(0)$ turns it at time t into $\rho(t) = L[\rho(0), t]$. Here L is the decoherence superoperator[14], which can be shown to satisfy the following relation:

$$D(\alpha e^{-t/2T_c})L[\rho(0),t]D(-\alpha e^{-t/2T_c}) = L[D(\alpha)\rho(0)D(-\alpha),t]$$

Translating the initial field by α and letting it evolve over time t is equivalent to letting it evolve during that time and translating it by $\alpha\exp(-t/2T_c)$. We thus analyse the data obtained at time t as if they corresponded to a translation rescaled by $\exp(-t/2T_c)$. This is more efficient than letting the field evolve before translating it, because we exploit all the data of a long sequence instead of recording only a short time window for each delay. We have experimentally checked the equivalence between the two methods by comparing the results for one time delay and have verified that the reconstructed Schrödinger cat states are, within the effects of noise, undistinguishable.

Figure 4a shows four snapshots of the Wigner function of an odd Schrödinger cat at increasing times, clearly revealing decoherence. Although the classical components have hardly decayed after 50 ms,

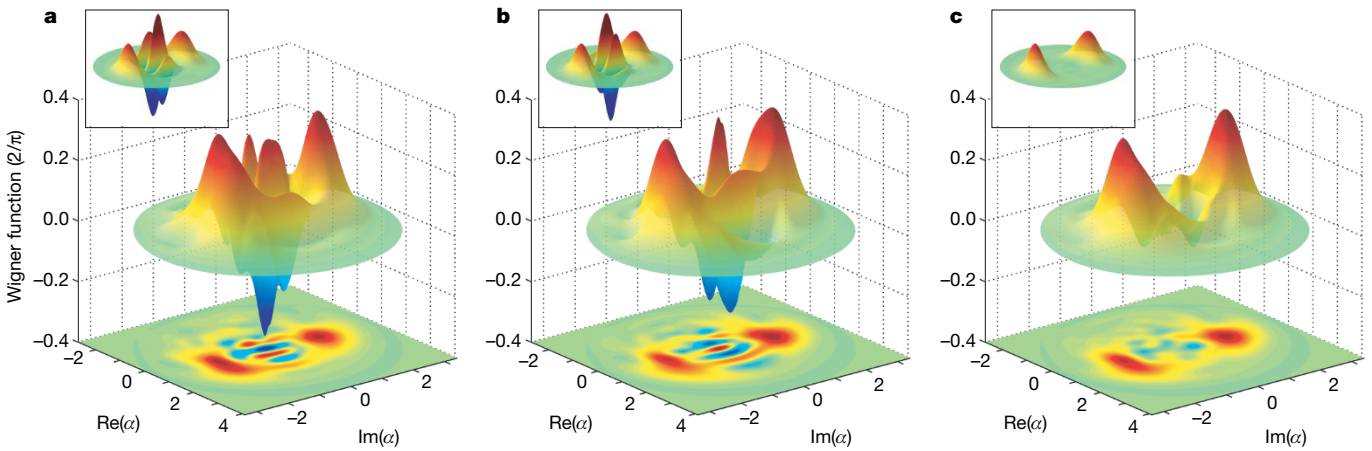

Figure 3 | Reconstructing Schrödinger cat states. **a**, **b**, The Wigner functions (in units of $2/\pi$) of even (**a**) and odd (**b**) Schrödinger cat states with $n_m = 3.5$ and $\chi = 0.37\pi$ are reconstructed, following state preparation. The same detuning ($\delta/2\pi = 51$ kHz) and interferometer phase ($\phi = -\Phi(0,\delta) + \pi$) are used for state preparation and reconstruction. The number of sampling points is ~500, with ~2,000 atoms detected at each point, in 400 realizations. The dimension of the Hilbert space used for reconstruction is 11. The small insets present for comparison the theoretical Wigner functions computed in the case of ideal preparation and detection of the atomic state superpositions. Decoherence during state preparation is taken into account. The maximum theoretical values of the classical components and interference fringes are close to 0.5 and 1, respectively. In the reconstructed states, the quantum interference is smaller, mainly owing to imperfections of the Ramsey interferometer that affect the preparation of the Schrödinger cat state (but not its reconstruction). **c**, Reconstructed Wigner function of the field prepared in C when the state of the preparation atom is not read-out (statistical mixture of two classical fields). Inset, corresponding theoretical Wigner function.

the interference feature has vanished, turning the initial state into a statistical mixture similar to that shown in Fig. 3c. A complete movie of the evolution of the Wigner function of a Schrödinger cat state is presented in the Supplementary Information. By subtracting the Wigner functions of the even and odd Schrödinger cat states corresponding to the same preparation sequence, we isolate their interference features by cancelling their equal, classical, parts. A movie showing the progressive vanishing of this interference is also provided in the Supplementary Information.

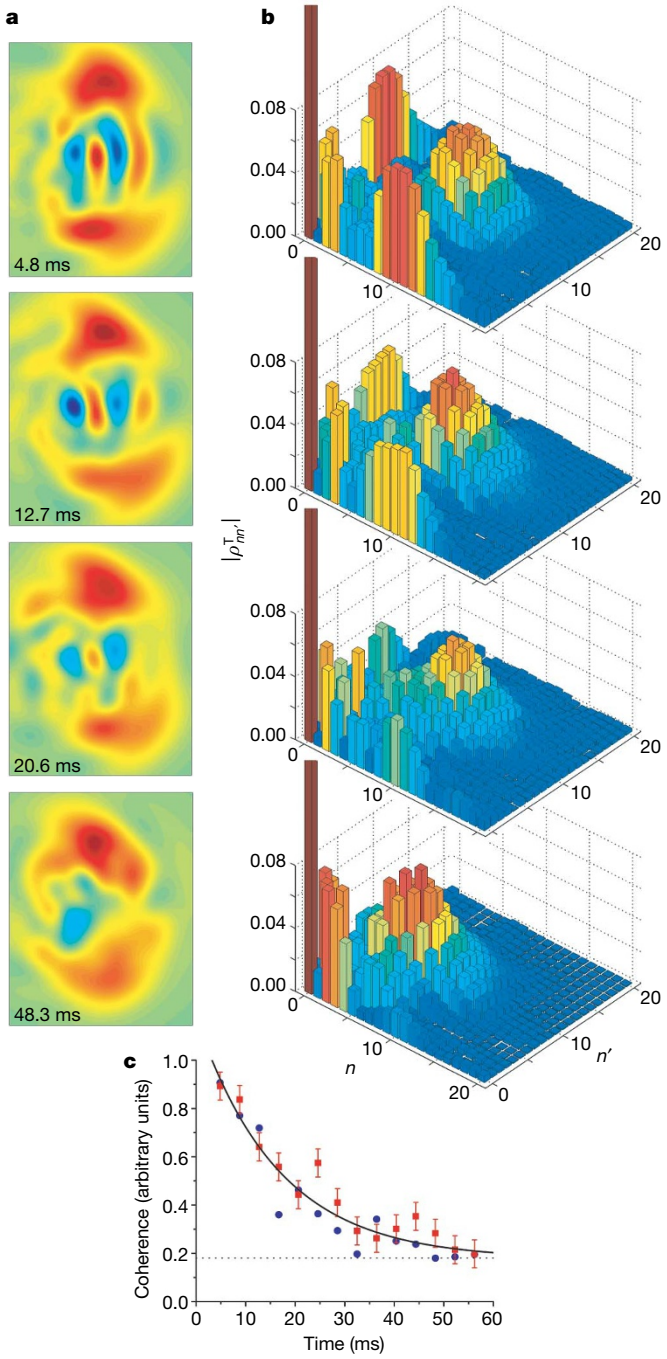

Figure 4 | Movie of decoherence. a, Snapshots of the Wigner function of the odd Schrödinger cat state in Fig. 3b at four successive times after state preparation. **b**, Corresponding snapshots of the translated density matrix ρ^{T} (modulus of matrix elements). The dimension of the Hilbert space is enlarged to 30. The $n = 0$ peak is clipped, its amplitude being ~0.38 in each snapshot. In all frames, the small matrix elements for $n < 5$ are due to the deviation of the classical component of the Schrödinger cat state from an ideal coherent state. **c**, The quantum coherence of the Schrödinger cat states (even, red; odd, blue), defined as the sum of the $|\rho^{T}_{n0}|$ for $n \geq 5$, plotted as a function of time. The statistical error bars (shown, for clarity, for the even Schrödinger cat states only) are obtained by analysing the state reconstructions performed on different subsamples of measured data. The solid line is a common exponential fit, including an offset (dotted line) accounting for residual noise in the modulus of the density matrix elements.

It is also instructive to observe decoherence directly in the density matrix. To distinguish the classical coherence of each component of the Schrödinger cat state from their mutual quantum coherence, we consider the mathematically translated reconstructed density matrix $\rho^{T} = \rho^{-\beta\exp(i\chi)}$, whose classical components are close to the vacuum $|0\rangle$ and to $|-2i\beta\sin\chi\rangle$. This formal translation leaves unchanged the distance between the two classical components in the phase plane as well as their mutual coherence.

In Fig. 4b, we present the density matrix $\rho^{T}(t)$ of the Schrödinger cat state in Fig. 4a, reconstructed for the same times. In each frame, the diagonal elements present two maxima around $n = 0$ and $n = 11$. The off-diagonal elements are of two kinds. Those for which $|n - n'| \approx \sqrt{11}$ describe the classical coherence of the non-vacuum component and remain nearly unchanged on the observed timescale. The off-diagonal terms in the first row and column of the matrix (respectively ρ^{T}_{0n} and ρ^{T}_{n0}) initially exhibit a bell-shaped variation with n, centred at $n \approx 11$. These terms correspond to the quantum coherence of the Schrödinger cat state responsible for the oscillations observed in the Wigner function. Their fast decay is the signature of decoherence.

The measured quantum coherence of the even and odd Schrödinger cat states is plotted as a function of time in Fig. 4c. A common exponential fit yields a decoherence time of $T_d = 17 \pm 3$ ms. A simple analytical model of decoherence[14] predicts that $T_d = 2T_c/d^2 = 22$ ms at $T = 0$ K, reduced to[24] $T_d = 2T_c/(d^2(1+2n_b)+4n_b) = 19.5$ ms when including a thermal background at $T = 0.8$ K, in good agreement with the measured value. A movie of a smaller Schrödinger cat state ($d^2 = 8$) yields $T_d = 28$ ms, illustrating the dependence of the decoherence time on the Schrödinger cat state size[5,14]. Earlier experiments have studied the relaxation of photonic[22] and atomic[25] Schrödinger cat states by observing some of their specific features, but this experiment allows us to produce a movie of decoherence in a fully reconstructed Schrödinger cat state.

We have shown that atoms interacting with a cavity field can be used to engineer and reconstruct a wide variety of photonic states and to study their evolution. Going one step farther, we plan to use information provided by the atoms to implement feedback procedures and preserve the quantum coherence over longer time intervals[26]. We will also extend these studies to fields stored in two cavities. Atoms will be used to entangle the cavity fields into non-local quantum states[27,28], reconstruct these states and protect them against decoherence by means of quantum feedback operations.

Received 25 June; accepted 23 July 2008.

1. Paris, M. G. A. & Řeháček, J. (eds) *Quantum State Estimation* (Springer, 2004).
2. Smithey, D. T., Beck, M., Raymer, M. G. & Faridani, A. Measurement of the Wigner distribution and the density matrix of a light mode using optical homodyne tomography: Application to squeezed states and the vacuum. *Phys. Rev. Lett.* **70**, 1244–1247 (1993).
3. Dunn, T. J., Walmsley, I. A. & Mukamel, S. Experimental determination of the quantum-mechanical state of a molecular vibrational mode using fluorescence tomography. *Phys. Rev. Lett.* **74**, 884–887 (1995).
4. Kurtsiefer, C., Pfau, T. & Mlynek, J. Measurement of the Wigner function of an ensemble of helium atoms. *Nature* **386**, 150–153 (1997).
5. Zurek, W. Decoherence, einselection, and the quantum origins of the classical. *Rev. Mod. Phys.* **75**, 715–775 (2003).
6. Leibfried, D. *et al.* Experimental determination of the motional quantum state of a trapped atom. *Phys. Rev. Lett.* **77**, 4281–4285 (1996).
7. Häffner, H. *et al.* Scalable multiparticle entanglement of trapped ions. *Nature* **438**, 643–646 (2005).
8. Morinaga, M., Bouchoule, I., Karam, J.-C. & Salomon, C. Manipulation of motional quantum states of neutral atoms. *Phys. Rev. Lett.* **83**, 4037–4040 (1999).
9. Glauber, R. J. Coherent and incoherent states of the radiation field. *Phys. Rev.* **131**, 2766–2788 (1963).

10. Bužek, V. & Knight, P. L. Quantum interference, superposition states of light, and nonclassical effects, in *Progress in Optics XXXIV* (ed. Wolf, E.) 1–158 (Elsevier, 1995).
11. Schleich, W. P. *Quantum Optics in Phase Space* (Wiley, 2001).
12. Kuhr, S. *et al.* Ultrahigh finesse Fabry-Pérot superconducting resonator. *Appl. Phys. Lett.* **90,** 164101 (2007).
13. Raimond, J.-M., Brune, M. & Haroche, S. Colloquium: manipulating quantum entanglement with atoms and photons in a cavity. *Rev. Mod. Phys.* **73,** 565–582 (2001).
14. Haroche, S. & Raimond, J.-M. *Exploring the Quantum: Atoms, Cavities and Photons* (Oxford Univ. Press, 2006).
15. Guerlin, C. *et al.* Progressive field state collapse and quantum non-demolition photon counting. *Nature* **448,** 889–893 (2007).
16. Bužek, V. & Drobny, G. Quantum tomography via the *MaxEnt* principle. *J. Mod. Opt.* **47,** 2823–2839 (2000).
17. Lutterbach, L. G. & Davidovich, L. Method for direct measurement of the Wigner function in cavity QED and ion traps. *Phys. Rev. Lett.* **78,** 2547–2550 (1997).
18. Lvovsky, A. I. *et al.* Quantum state reconstruction of the single-photon Fock state. *Phys. Rev. Lett.* **87,** 050402 (2001).
19. Zavatta, A., Viciani, S. & Bellini, M. Tomographic reconstruction of the single-photon Fock state by high-frequency homodyne detection. *Phys. Rev. A* **70,** 053821 (2004).
20. Ourjoumtsev, A., Tualle-Brouri, R. & Grangier, P. Quantum homodyne tomography of a two-photon Fock state. *Phys. Rev. Lett.* **96,** 213601 (2006).
21. Bertet, P. *et al.* Direct measurement of the Wigner function of a one-photon Fock state in a cavity. *Phys. Rev. Lett.* **89,** 200402 (2002).
22. Brune, M. *et al.* Observing the progressive decoherence of the 'meter' in a quantum measurement. *Phys. Rev. Lett.* **77,** 4887–4890 (1996).
23. Ourjoumtsev, A., Jeong, H., Tualle-Brouri, R. & Grangier, P. Generation of optical 'Schrödinger cats' from photon number states. *Nature* **448,** 784–786 (2007).
24. Kim, M. S. & Bužek, V. Schrödinger cat states at finite temperature: Influence of a finite temperature heat bath on quantum interferences. *Phys. Rev. A.* **46,** 4239–4251 (1992).
25. Myatt, C. J. *et al.* Decoherence of quantum superpositions through coupling to engineered reservoirs. *Nature* **403,** 269–273 (2000).
26. Zippilli, S., Vitali, D., Tombesi, P. & Raimond, J.-M. Scheme for decoherence control in microwave cavities. *Phys. Rev. A* **67,** 052101 (2003).
27. Davidovich, L., Brune, M., Raimond, J.-M. & Haroche, S. Mesoscopic quantum coherences in cavity QED: preparation and decoherence monitoring schemes. *Phys. Rev. A* **53,** 1295–1309 (1996).
28. Milman, P. *et al.* A proposal to test Bell's inequalities with mesoscopic non-local states in cavity QED. *Eur. Phys. J. D* **32,** 233239 (2005).

Supplementary Information is linked to the online version of the paper at www.nature.com/nature.

Acknowledgements This work was supported by the Agence Nationale pour la Recherche (ANR), by the Japan Science and Technology Agency (JST) and by the European Union under the Integrated Projects SCALA and CONQUEST. S.D. is funded by the Délégation Générale pour l'Armement (DGA).

Author Contributions S.D., I.D. and C.S. contributed equally to this work.

Author Information Reprints and permissions information is available at www.nature.com/reprints. Correspondence and requests for materials should be addressed to S.H. (haroche@lkb.ens.fr).